

Eddy diffusivity near bubble plumes

Danielle J. Wain and Chris R. Rehmann

Department of Civil, Construction, and Environmental Engineering, Iowa State University, Ames, Iowa, USA

Received 13 December 2004; revised 6 May 2005; accepted 16 May 2005; published 14 September 2005.

[1] Profiles of eddy diffusivity and the rate of dissipation of temperature variance were inferred from temperature microstructure measurements near a bubble plume at the center of a tank with a diameter of 13.7 m and a maximum depth of 8.3 m. Measurements occurred outside the bubbly part of the flow. Profiles of eddy diffusivity were estimated with two methods: one based on the equation for turbulent kinetic energy and one based on the equation for temperature variance. The eddy diffusivities showed nonmonotonic behavior with distance from the plume axis, as in numerical simulations. Eddy diffusivities estimated with the two methods match well, except for one data set with strong turbulence and weak stratification. The estimates of the eddy diffusivity allow two empirical formulas for the bulk, or tank-averaged, effective diffusivity to be evaluated; the bulk diffusivity is within the range of values predicted by the models.

Citation: Wain, D. J., and C. R. Rehmann (2005), Eddy diffusivity near bubble plumes, *Water Resour. Res.*, 41, W09409, doi:10.1029/2004WR003896.

1. Introduction

[2] Bubble plumes are used to manage water quality in lakes and reservoirs. By aerating the water and breaking up the stratification, they provide several ecological and water quality benefits. Disrupting the thermal stratification can improve the quality of water removed from reservoirs through selective withdrawal [Imberger and Patterson, 1990]. The increased circulation and aeration can promote the growth of grazing zooplankton [e.g., Field and Prepas, 1997] and prevent fish kills caused by lack of oxygen [e.g., Ellis and Stefan, 1991]. Bubble plumes can also be used in wastewater reservoirs. For example, operators of McCook Reservoir, which is designed to capture and store nearly 3×10^7 m³ of combined sewage in the Chicago (USA) area, plan to use bubble plumes to mix and aerate the sewage. In this case, bubble plumes can help aerobic bacteria eliminate odors caused by decaying matter [e.g., Heo and Kim, 2004] and agitate the sludge to keep it from settling to the bottom [e.g., McGhee, 1991, p. 463]. To improve the understanding of mixing and transport in flows with bubble plumes, we present estimates of the eddy diffusivity, which can be used to evaluate empirical diffusivity formulas and turbulence models.

[3] In the design of mixing and aeration systems for applications in water resources, bubble plumes are often modeled with one-dimensional integral models [e.g., Schladow, 1992; Wüest et al., 1992], but models that include a more detailed description of the turbulence have been proposed. For example, Bernard et al. [2000] used the k - ϵ model, in which the turbulent kinetic energy k and its dissipation rate ϵ are computed and used to calculate eddy viscosity and diffusivity to close the equations for the mean quantities. Researchers often use the standard k - ϵ model to model the two-phase flow, but others add extra terms to the equations for k and ϵ to account for turbulence generated by

bubbles [e.g., Sheng and Irons, 1993; Smith, 1998]. Although bubble-induced turbulence can be large in parts of the plume, in much of a dilute plume, bubbles increase the eddy diffusivity by a small amount; nevertheless, bubble-induced turbulence couples the plume more strongly to the ambient fluid and therefore affects the mixing of the water body [Smith, 1998].

[4] Without turbulence measurements in flows driven by bubble plumes, modifications to turbulence models cannot be validated. Some researchers have measured turbulent kinetic energy and Reynolds stress in bubble plumes [Iguchi et al., 1995; Grevet et al., 1982], and recently, Soga and Rehmann [2004] (hereinafter referred to as SR) measured the dissipation of turbulent kinetic energy. Because applications of bubble plumes involve mixing and transport, an important quantity to measure and predict is the eddy diffusivity, which is used to model vertical fluxes. For example, the temperature flux F_T can be written as

$$F_T = -K_T \frac{\partial T}{\partial z}, \quad (1)$$

where K_T is the eddy diffusivity of temperature T and z is the vertical coordinate. Parameterizations of the bulk (or tank-averaged) eddy diffusivity are available, and turbulence models can predict the spatial variation of eddy diffusivity. However, measurements that can be used to verify model predictions are lacking. Iguchi and Morita [1992] determined the effective diffusivity (i.e., the sum of the molecular and eddy diffusivities) of bubbles in a small vessel from measurements of gas holdup and mean velocity, but applying their results to large water bodies is difficult.

[5] To provide a data set that can be used to evaluate parameterizations of turbulence in flows driven by bubble plumes, we use measurements of the small-scale temperature field to compute dissipation rates and estimate eddy diffusivities in a weakly stratified flow. We extend the calculations of SR by computing the dissipation of scalar variance $\chi_T = 2D_T(\nabla T')^2$, where D_T is the molecular

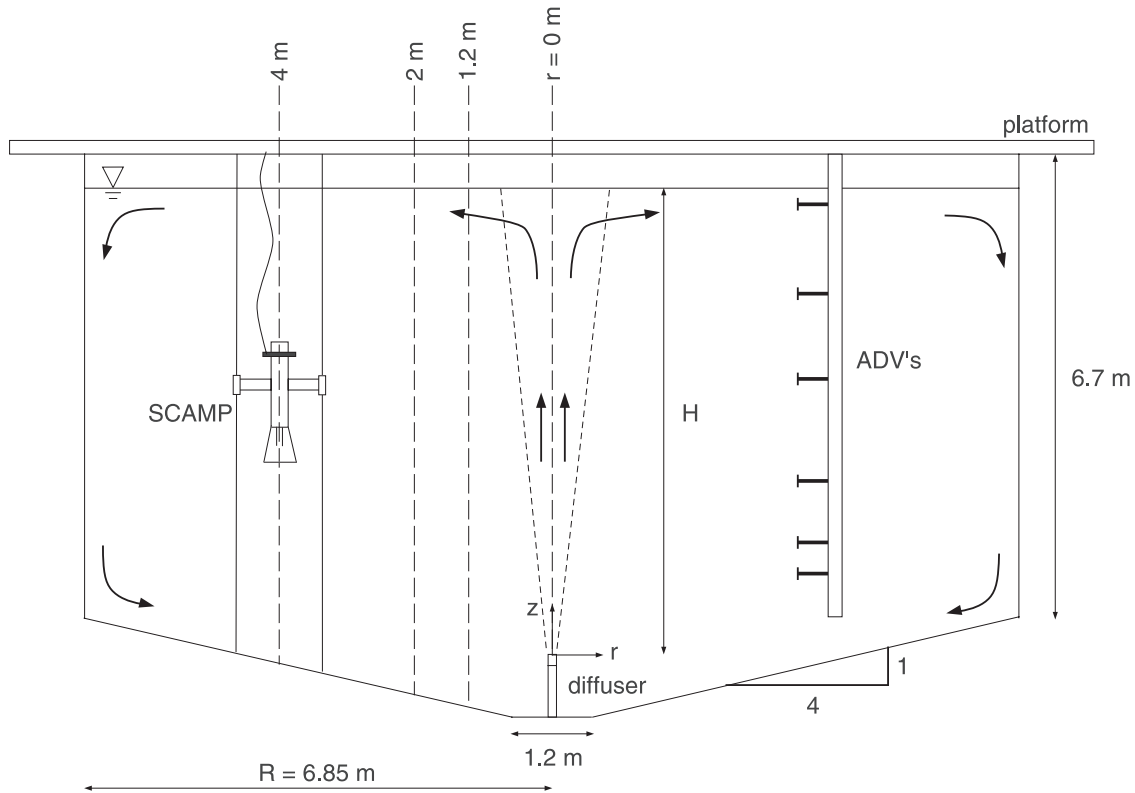


Figure 1. Schematic of the experimental facility, measurement locations, and flow patterns. For data sets 1 and 2 the SCAMP and cable assembly were oriented as shown. For the other data sets the assembly was rotated to be perpendicular to the plane.

diffusivity of temperature and T' is the temperature fluctuation. We use methods based on the equations for temperature variance and turbulent kinetic energy to estimate eddy diffusivities K_T and K_ρ of temperature and density as

$$K_T = \frac{\chi_T}{2(\partial\bar{T}/\partial z)^2} \quad \text{and} \quad K_\rho = \Gamma \frac{\epsilon}{N^2}, \quad (2)$$

where \bar{T} is the mean temperature, Γ is a coefficient, and N is the buoyancy frequency. After summarizing the experimental procedures in section 2, we describe the calculation of eddy diffusivity in detail in section 3. We present dissipation and eddy diffusivity profiles, compare the two estimates of eddy diffusivity in (2), and evaluate bulk parameterizations and results from previous numerical studies in section 4. The main conclusions are summarized in section 5. Along with the work of SR, our calculations form a baseline set of measurements of dissipation and eddy diffusivity against which turbulence models can be compared.

2. Experiment

[6] Because SR provide full details of the experiments, only a brief description is given here. Experiments were conducted in a tank at a sewage treatment plant with a diameter of 13.7 m, a depth at the walls of 6.7 m, a depth at the center of 8.3 m, and a volume of 1075 m³ (Figure 1). The bubble plume was created by forcing compressed air through a stainless steel, commercially available coarse-

bubble air diffuser placed 0.95 m above the bottom in the center of the tank. The diffuser was 0.6 m long, and its axis was perpendicular to the plane of the measurements. The diffuser has twelve 5-mm circular openings, twelve 10-mm circular openings, and two 11-mm slots that run the length of the diffuser on either side. Airflow rates Q_H at standard pressure and temperature ranged from 0.1 to 0.6 L s⁻¹. The water depth H above the diffuser was 7 m. Heating from the sun established the background temperature gradient (see SR, their Figure 2), which weakened as experiments progressed. The experimental conditions are listed in Table 1.

[7] Temperature microstructure was measured with the self-contained autonomous microprofiler (SCAMP) manufactured by Precision Measurement Engineering. The SCAMP measures small-scale temperature fluctuations with Thermometrics FP07 thermistors, which have a nominal response time of 7 ms, though the actual response depends on probe speed and sensor construction [Gregg, 1999]. The SCAMP was attached to cables that kept it at a fixed radial distance from the bubble plume's axis and allowed it to fall through the water column at a rate measured with a pressure sensor in the SCAMP. In the experiments, the fall rate was approximately 0.1 m s⁻¹, and temperatures were recorded at 100 Hz. Analog signal processors in the SCAMP computed the time derivative of the voltage signals from the thermistors before the signals were digitized. After accounting for vertical water velocities measured with acoustic Doppler velocimeters, temperature gradient profiles were computed with Taylor's hypothesis [e.g., Tennekes and Lumley, 1989,

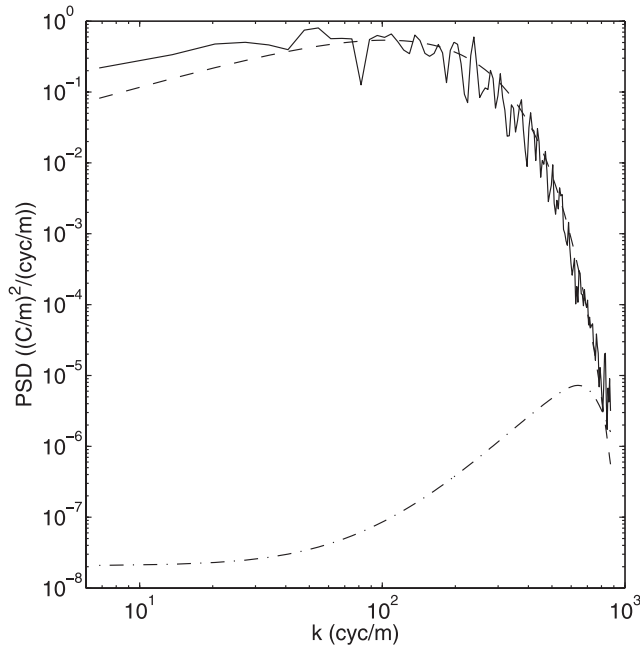


Figure 2. Example of a fit of the Batchelor spectrum (dashed line) to a measured temperature gradient spectrum (solid line). The SCAMP's noise spectrum is shown by a dash-dotted line.

p. 253]. The temperature gradients were then used to compute dissipation and eddy diffusivity.

3. Processing

[8] SR computed the dissipation of turbulent kinetic energy by fitting a theoretical form of the temperature gradient spectrum, originally derived by *Batchelor* [1959], to the observed data. The one-dimensional spectrum $S_B(k_1)$ of the temperature gradient is

$$S_B(k_1) = \sqrt{\frac{q}{2}} \frac{\chi_T}{D_T k_B} \kappa \left(e^{-\kappa^2/2} - \kappa \int_{\kappa}^{\infty} e^{-x^2/2} dx \right), \quad (3)$$

where k_1 is the wave number, D_T is the diffusivity of temperature, and q is a constant, taken here to be 3.4 [Ruddick et al., 2000]. The Batchelor wave number is $k_B = (\epsilon/\nu D_T^2)^{1/4}$, where ν is the kinematic viscosity of the fluid, and $\kappa = (2q)^{1/2} k_1/k_B$. The dissipation of temperature variance was estimated directly by assuming isotropy and integrating the difference of the observed spectrum S_{obs} and the noise spectrum S_n of the SCAMP over all wave numbers:

$$\chi_T = 6D_T \int [S_{obs}(k_1) - S_n(k_1)] dk_1. \quad (4)$$

Then the theoretical Batchelor spectrum was fit to measured temperature gradient spectra at high wave numbers by adjusting the single free parameter k_B (Figure 2). From the best fit, the dissipation ϵ was estimated from the definition of the Batchelor wave number. SR implemented this procedure by dividing each profile into segments of about 0.5 m and fitting the Batchelor spectrum with the method of

Ruddick et al. [2000]. Segments with poorly fitting spectra were discarded according to the criteria recommended by Ruddick et al. [2000]. Dissipation values were assigned to 0.25 m intervals in the vertical domain, and the mean profiles of ϵ and χ_T were computed as the mean of 200 bootstrap resampled populations [e.g., Efron and Tibshirani, 1993].

[9] Eddy diffusivities were estimated with two methods used in oceanography [e.g., Osborn and Cox, 1972; Osborn, 1980]. The first method uses the equation for temperature variance:

$$\frac{\partial}{\partial t} \left(\frac{1}{2} \overline{T'^2} \right) + U_j \frac{\partial}{\partial x_j} \left(\frac{1}{2} \overline{T'^2} \right) = -\overline{T'w'} \frac{\partial \overline{T}}{\partial z} - \frac{1}{2} \chi_T - \frac{\partial}{\partial x_j} \left[\frac{1}{2} \overline{T'^2 u'_j} - D_T \frac{\partial}{\partial x_j} \left(\frac{1}{2} \overline{T'^2} \right) \right], \quad (5)$$

where U_j is the mean velocity and u'_j is the fluctuating velocity. The production and dissipation terms are usually assumed to balance each other [e.g., Osborn and Cox, 1972]:

$$-\overline{T'w'} \frac{\partial \overline{T}}{\partial z} = \frac{1}{2} \chi_T, \quad (6)$$

where w is the vertical velocity and z is the vertical coordinate. Then using the flux-gradient relationship $\overline{T'w'} = -K_T \partial \overline{T} / \partial z$ in (6) yields

$$K_T = \frac{\chi_T}{2(\partial \overline{T} / \partial z)^2}. \quad (7)$$

We discuss the validity of (7) for our flow below.

[10] The second method uses the turbulent kinetic energy equation:

$$\frac{\partial k}{\partial t} + U_j \frac{\partial k}{\partial x_j} = -\frac{\partial J_j}{\partial x_j} - \overline{u'_i u'_j} \frac{\partial U_i}{\partial x_j} - b - \epsilon, \quad (8)$$

where J_j is a flux of turbulent kinetic energy, $b = g\overline{\rho'w'}/\rho_0$ is the buoyancy flux, g is the acceleration due to gravity, and ρ_0 is a reference density. For oceanic flows, the last three terms are assumed to balance [e.g., Osborn, 1980]. For more general flows, Ivey and Imberger [1991] wrote (8) as

Table 1. Experimental Conditions

Data Set	Q_{ns}^a L s ⁻¹	$r,^b$ m	Number of Profiles	Percent of Segments Rejected		
				Poor Fit	$\partial \overline{T} / \partial z < 0$	Mean $\epsilon/\nu N^2$
1	0.1	2.0	18	13	50	14,000
2	0.1	4.0	18	3	33	1400
3 ^c	0.2	1.2	51	4	27	1700
4	0.2	2.0	33	6	52	10,000
5 ^c	0.2	4.0	42	9	38	1100
6	0.6	4.0	39	3	48	42,000

^aAirflow rate at the free surface.

^bRadial distance from the plume axis at which the profiles were measured.

^cFive profiles in both data sets 3 and 5 were discarded after analyzing the validity of equation (7) for these experiments.

$m = b + \epsilon$. Using the generalized flux Richardson number $R_f = b/m$ and the flux-gradient relationship $\overline{\rho'w'} = -K_p \partial \bar{\rho} / \partial z$ gives

$$K_p = \frac{R_f}{1 - R_f} \frac{\epsilon}{N^2} = \Gamma \frac{\epsilon}{N^2}, \quad (9)$$

where $N = [-(g/\rho_0) \partial \bar{\rho} / \partial z]^{1/2}$ is the buoyancy frequency and $\Gamma = R_f / (1 - R_f)$. Because the density in our flow depended on temperature only, the temperature gradient was used to calculate the buoyancy frequency:

$$N^2 = -\frac{g}{\rho_0} \frac{\partial \bar{\rho}}{\partial z} = g\beta \frac{\partial \bar{T}}{\partial z}, \quad (10)$$

where β is the thermal expansion coefficient of water calculated from the equation of state of *Ruddick and Shirtcliffe* [1979].

[11] The mean temperature gradient $\partial \bar{T} / \partial z$ was determined by fitting a line to the temperature data in each segment. The expansion coefficient β was computed from the average temperature in each segment. The temperature and temperature gradient profiles were then divided into 0.25 m intervals, and the mean profiles were obtained by a bootstrap mean as described above. Data from segments with unstable temperature gradients (i.e., $\partial \bar{T} / \partial z < 0$) were discarded prior to averaging. These mean values and the bootstrapped mean and 95% confidence limits for ϵ and χ_T were used to compute profiles of K_T and K_p and their 95% confidence limits.

[12] Uncertainty in the eddy diffusivity K_T computed with (7) comes from the assumption of isotropy, the fit of the mean temperature gradient for each segment, the resolution of χ_T , and the validity of the production-dissipation balance for this flow. Uncertainty due to the assumption of isotropy is about 3% (SR). An analysis of the robust linear fit used to compute the temperature gradient yields an uncertainty of approximately 15% in $\partial \bar{T} / \partial z$. More than 95% of χ_T is resolved in all spectra before they meet the noise spectrum. Attenuation of the thermistor response [e.g., *Gregg*, 1999] is small for a profiling speed of 0.1 m/s and the lower values of dissipation observed [*Rehmann et al.*, 2004], and effects of thermistor response can be corrected to within 12% for all values of dissipation measured. *Wain and Rehmann* [2005] evaluated the validity of equation (7) by estimating the relative importance of terms in (4). The contribution of the neglected terms mostly falls within the likely measurement uncertainty: Effects of unsteadiness are largest in the bottom 2 m of data set 3. Also, we did not compute K_T in the top 1 m of all profiles because vertical advection was large there.

[13] Uncertainty in estimating the eddy diffusivity K_p computed with (9) comes mainly from uncertainty in the value used for Γ and the dissipation ϵ . We take $\Gamma = 0.2$, although it can vary with stratification strength and the process generating the turbulence [e.g., *Ivey and Imberger*, 1991]. For example, in oceanographic measurements it varies as a function of the parameter $\epsilon/\nu N^2$ [*Ruddick et al.*, 1997]. We assign a 50% uncertainty to the value 0.2 but also discuss possible variations in Γ in section 4.2. Potential sources of uncertainty in estimating ϵ include sensor resolution, anisotropy, vertical currents, the spectral fit, and the

validity of the Batchelor spectrum. SR and *Rehmann et al.* [2004] discussed and quantified these sources of uncertainty, though computing overall uncertainty in ϵ is difficult because of issues such as the validity of the Batchelor spectrum. As reassurance, however, we note that our estimates of ϵ match those from the ADV measurements, themselves subject to uncertainty, within a factor of 2 [*Rehmann et al.*, 2004].

4. Results and Discussion

[14] After briefly summarizing the results of SR for dissipation of turbulent kinetic energy, we present and discuss profiles and trends of dissipation of temperature variance. We present and compare the profiles of eddy diffusivity calculated by both (7) and (9). We discuss the magnitude and the shape of the profiles and trends of the eddy diffusivity with radius and airflow rate. Finally, we evaluate models for the bulk effective viscosity and compare our measurements with results from numerical simulations of bubble plumes.

4.1. Dissipation Rates

[15] Table 1 shows the percentage of segments that were rejected as described. Only data set 1 had more than 10% of its segments rejected because of the quality of the spectral fit. Between 27% and 52% of the segments were omitted from further analysis because of unstable temperature gradients, which are due to the bubble plume either creating local overturns or advecting cold water from the bottom of the tank. Almost all of the segments in the upper 0.5 m of all data sets, which were discarded because of large vertical advection of T'^2 , had a persistent unstable temperature profile near the water surface. Consequently, the percentage rejected in the interior of the water column was smaller.

[16] SR found the averaged dissipation of turbulent kinetic energy for all the data sets to be between 10^{-8} and $10^{-6} \text{ m}^2 \text{ s}^{-3}$ for most of the profile. These values were much smaller than the tank-averaged rate of work done by the bubble plume because much of the dissipation occurs in the bubble plume and some of the plume's energy is used to create waves on the free surface (SR). Some of the vertical variation in dissipation is due to the large-scale flow, which is sketched in Figure 1. SR attributed the sharp increase in dissipation at the surface to shear associated with the surface outflow. This increase can be seen in numerical studies of bubble plumes [e.g., *Sheng and Irons*, 1993]. The dissipation rate mainly increased with flow rate and decreased with distance from the plume; however, for high flow rate and large radius, the dissipation increased near the bottom, possibly because of shear from the recirculating return flow. The latter observation would probably not apply to isolated bubble plumes in large lakes, but it could be relevant to reservoirs, such as McCook Reservoir, with arrays of diffusers.

[17] The averaged profiles of dissipation of temperature variance are shown in Figure 3. Figures 3a and 3b show averaged profiles at airflow rates of 0.1 L s^{-1} and 0.2 L s^{-1} , respectively, while Figure 3c shows averaged profiles at a radius of 4 m from the center of the plume for the three different airflow rates. The normalized confidence limits for the data sets with the smallest (data set 6) and largest (data set 1) confidence intervals are shown in Figure 4. Measured

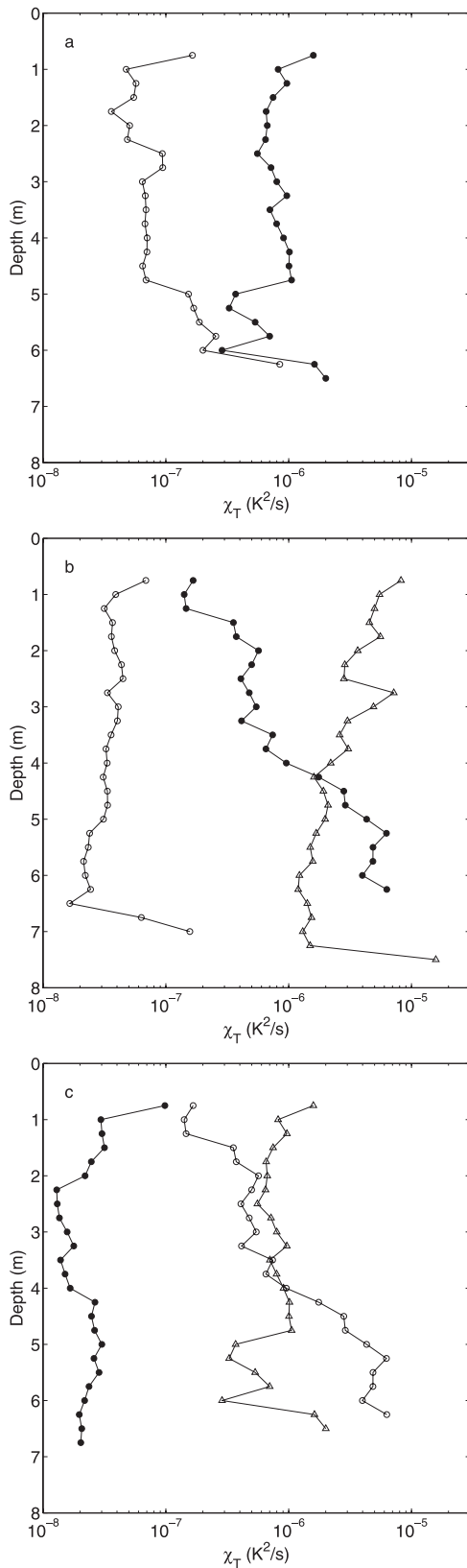


Figure 3. Averaged profiles of dissipation of temperature variance: (a) $Q_H = 0.1 \text{ L s}^{-1}$, (b) $Q_H = 0.2 \text{ L s}^{-1}$, and (c) $r = 4 \text{ m}$. For Figures 3a and 3b the data symbols are triangles, $r = 1.2 \text{ m}$; open circles, $r = 2 \text{ m}$; solid circles, $r = 4 \text{ m}$. For Figure 3c, the data symbols are triangles, $Q_H = 0.1 \text{ L s}^{-1}$; open circles, $Q_H = 0.2 \text{ L s}^{-1}$; solid circles, $Q_H = 0.6 \text{ L s}^{-1}$.

values of χ_T vary between 10^{-8} and $10^{-5} \text{ K}^2 \text{ s}^{-1}$. This range is similar to that found by *Sander et al.* [2000] for highly active turbulence in two lakes caused by strong winds and large surface buoyancy flux. *Rehmann and Duda* [2000] reported values between 10^{-7} and $10^{-5} \text{ K}^2 \text{ s}^{-1}$ near an oceanic front. The spatial variation of χ_T differs from that of ϵ because the dissipation of temperature variance depends on the temperature gradient, which itself varies with both depth and distance from the plume axis. In the experiments χ_T depended strongly on $\partial\bar{T}/\partial z$. The increase in χ_T with increasing $\partial\bar{T}/\partial z$ is expected since, for example, χ_T must be zero in a fluid with uniform temperature.

4.2. Eddy Diffusivity

[18] The averaged profiles of eddy diffusivity are shown in Figures 5–7. Figures 5 and 6 show the averaged profiles at airflow rates of 0.1 L s^{-1} and 0.2 L s^{-1} , respectively, while Figure 7 shows the averaged profiles at a radius of 4 m from the center of the plume for the three different airflow rates. The confidence intervals for K_ρ are smaller than those for K_T for all data sets (Figure 8).

[19] The calculated values of eddy diffusivity range between 10^{-5} and $10^{-2} \text{ m}^2 \text{ s}^{-1}$, or approximately 10^2 – 10^5 times the molecular diffusivity of temperature. The magnitude of the eddy diffusivity can also be compared to the eddy viscosities computed from the k - ϵ model as long as the two quantities are approximately equal. Although the eddy diffusivity and eddy viscosity can differ in strongly stratified flows, for weakly stratified flows, such as the bubble plumes in our experiments, the turbulent Prandtl number is approximately 1 [e.g., *Rodi*, 1987]. *Grevet et al.* [1982] and *Iguchi and Morita* [1992] reported values of the effective viscosity, which for large values is approximately equal to the eddy viscosity, of up to $O(10^{-4}) \text{ m}^2 \text{ s}^{-1}$, while

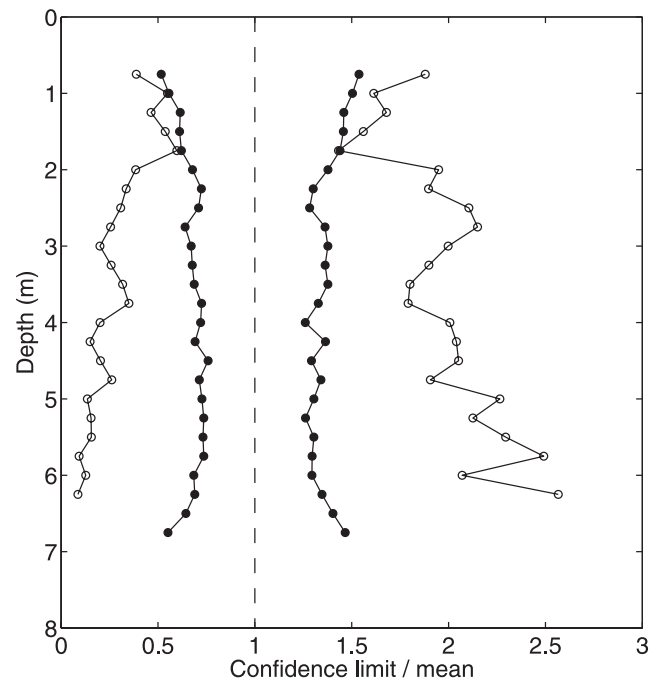


Figure 4. Normalized confidence limits for χ_T for the cases with the smallest (data set 6, solid circles) and largest (data set 1, open circles) intervals.

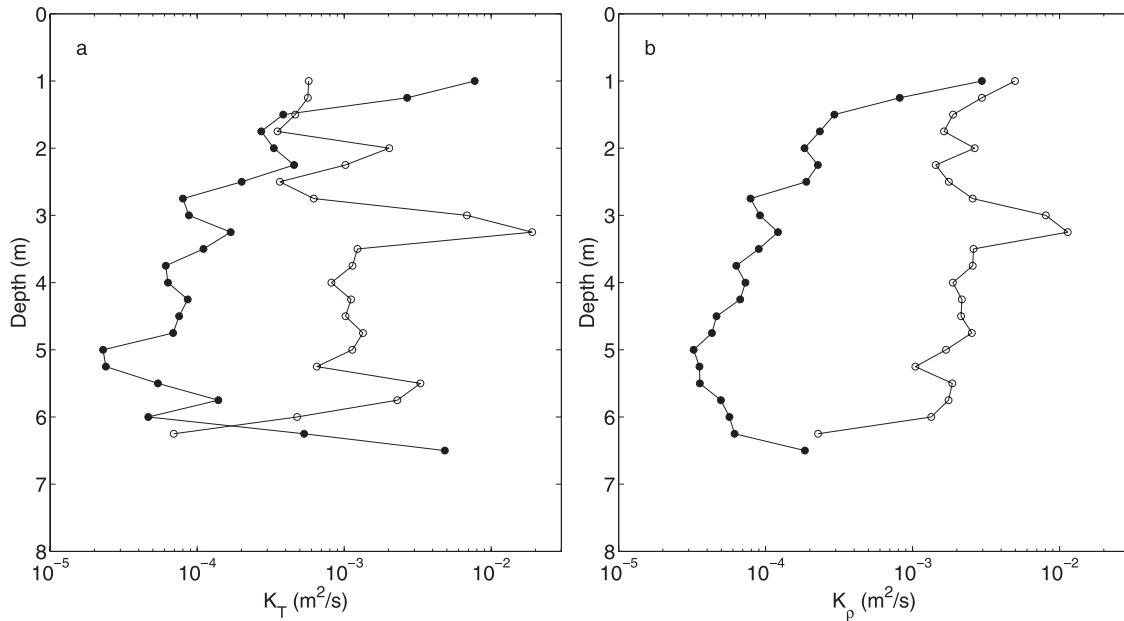


Figure 5. Averaged eddy diffusivity profiles for $Q_H = 0.1 \text{ L s}^{-1}$: (a) K_T and (b) K_ρ ($\Gamma = 0.2$). Open circles are $r = 2$ m, and solid circles are $r = 4$ m.

Sahai and Guthrie [1982b] found maximum effective viscosities of $10^{-1} \text{ m}^2 \text{ s}^{-1}$. Of course, the magnitude of the eddy diffusivity or eddy viscosity depends on the tank dimensions and airflow rate; these factors are incorporated into the analysis of bulk effective viscosity relationships below.

[20] When $Q_H = 0.1 \text{ L s}^{-1}$, the eddy diffusivity computed with both methods decreases with distance from the plume at most depths (Figure 5). When $Q_H = 0.2 \text{ L s}^{-1}$, profiles of K_T at the three radii and K_ρ at $r = 1.2$ and 4 m are equal within the uncertainty in the upper 4 m of the tank

(Figure 6). Below a depth of 4 m, K_T decreases between $r = 2$ and 4 m as for $Q_H = 0.1 \text{ L s}^{-1}$, and K_T at $r = 1.2$ m is even smaller. Results from numerical simulations show similar non-monotonic behavior of the eddy viscosity with distance from the plume axis [Grevet et al., 1982; Sahai and Guthrie, 1982b]. At $r = 4$ m K_T does not depend strongly on the flow rate above a depth of 4 m, though below that level K_T increases with flow rate (Figure 7). Values of K_ρ differ little for the two smaller flow rates, but when $Q_H = 0.6 \text{ L s}^{-1}$, the values, which were computed with $\Gamma = 0.2$, are much higher.

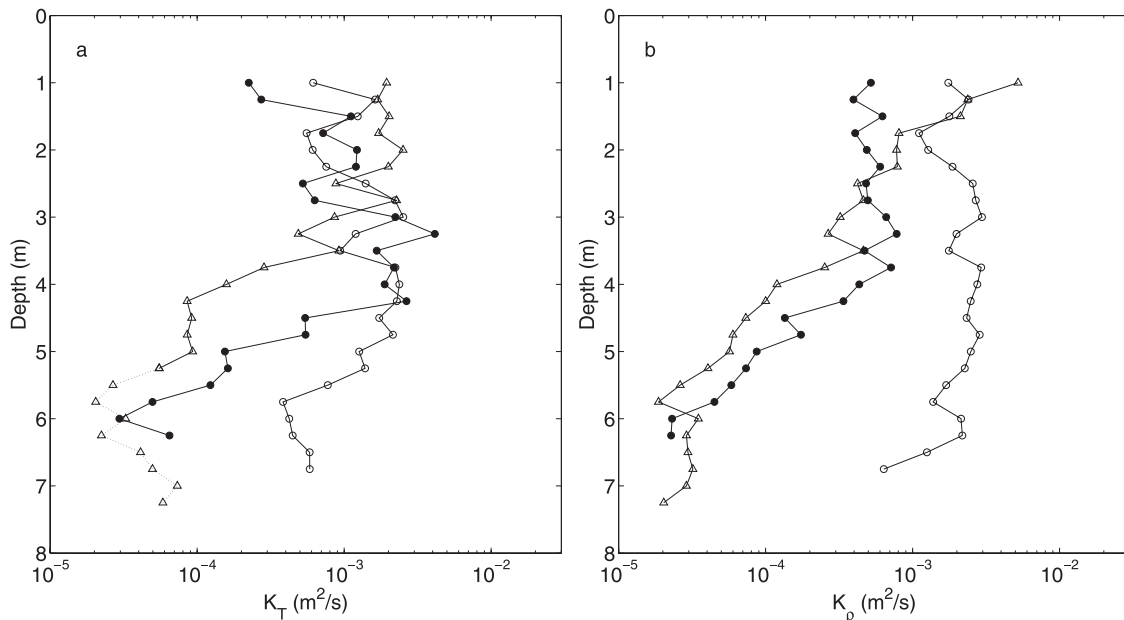


Figure 6. Averaged eddy diffusivity profiles for $Q_H = 0.2 \text{ L s}^{-1}$: (a) K_T and (b) K_ρ ($\Gamma = 0.2$). Symbols are triangles, $r = 1.2$ m; open circles, $r = 2$ m; solid circles, $r = 4$ m. The dashed line indicates the region in data set 3 where the flow may be nonstationary.

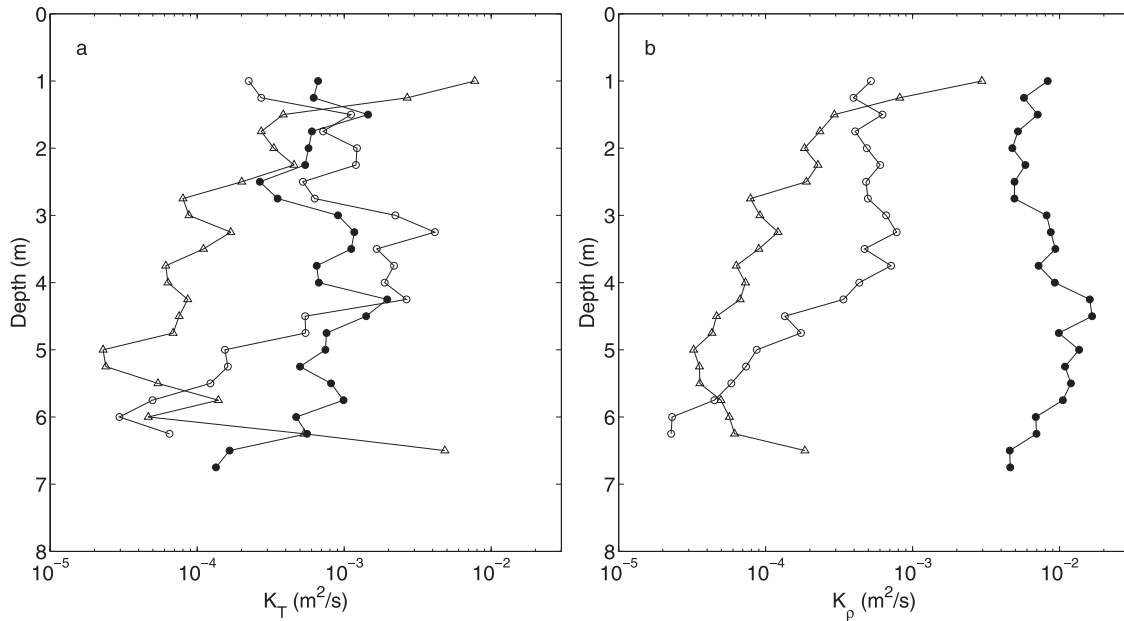


Figure 7. Averaged eddy diffusivity profiles for $r = 4$ m: (a) K_T and (b) K_ρ ($\Gamma = 0.2$). Symbols are triangles, $Q_H = 0.1 \text{ L s}^{-1}$; open circles, $Q_H = 0.2 \text{ L s}^{-1}$; solid circles, $Q_H = 0.6 \text{ L s}^{-1}$.

[21] In principle, K_T and K_ρ should be equal since the density differences in the experiments were due to temperature only. The eddy diffusivities K_ρ and K_T were equal within the confidence limits for most of the measurements, but K_ρ systematically exceeded K_T in data set 6 (Figure 9). Deviations of Γ from 0.2 could cause the differences between the eddy diffusivities; in particular, Γ would need to be smaller than 0.2 for the eddy diffusivities to match in experiment 6. This explanation is plausible because several studies have shown that mixing in a stratified fluid depends on, among other factors, the state of the turbulence, mea-

sured by the turbulent Froude number Fr_T , turbulent Reynolds number Re_T , or $\epsilon/\nu N^2$ [Ivey and Imberger, 1991]. In particular, data set 6 had large values of Fr_T (Figure 10), for which Γ is small [Ivey and Imberger, 1991] and the largest mean value of $\epsilon/\nu N^2$ (Table 1 and Figure 10). Laboratory measurements show that Γ decreases when $\epsilon/\nu N^2 > O(10^3)$ [Itsweire et al., 1986; Barry et al., 2001; Rehmann and Koseff, 2004], although measurements from

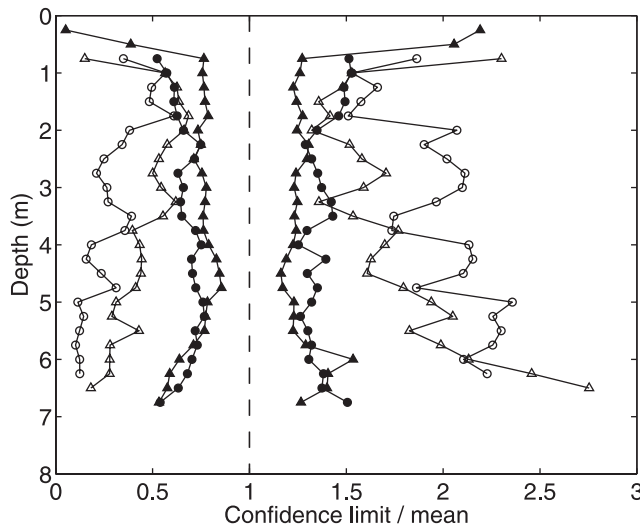


Figure 8. Normalized confidence limits for the data sets with the smallest and largest intervals for K_T (circles) and K_ρ (triangles). The data sets with the smallest intervals for K_T and K_ρ (solid symbols) were data sets 6 and 4, respectively, while the data sets with the largest intervals (open symbols) were data sets 1 and 2, respectively.

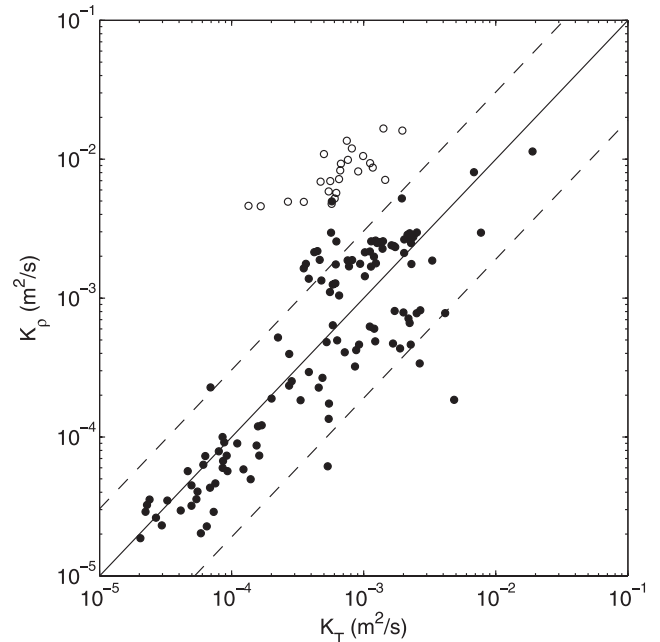


Figure 9. Comparison of the two eddy diffusivities K_T and K_ρ . Solid circles are data sets 1–5, and open circles are data set 6. The solid line represents $K_T = K_\rho$, and the dashed lines represent the average confidence intervals for the eddy diffusivity.

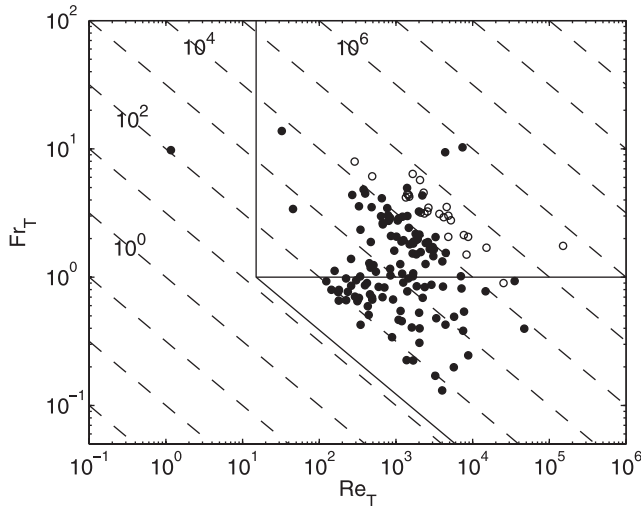


Figure 10. Location of the data in the Froude number–Reynolds number plane introduced by *Ivey and Imberger* [1991]. Solid circles are data sets 1–5, and open circles are data set 6. Values of $Fr_T = \epsilon^{1/3}/NL_i^{2/3}$ and $Re_T = \epsilon^{1/3}L_i^{4/3}/\nu$ were computed from the Ellison scale $L_i = (T'^2)^{1/2}/(\partial\bar{T}/\partial z)$. Dashed lines are contours of $\epsilon/\nu N^2$. Solid lines show $Fr_T = 1$ and the limits for active mixing, as determined by *Ivey and Imberger* [1991].

the upper ocean show the opposite trend [*Ruddick et al.*, 1997].

[22] The experimental estimates of the eddy diffusivity can be used to evaluate expressions for the bulk, or tank-averaged, effective viscosity. Bulk effective viscosity models developed by *Sahai and Guthrie* [1982a] and *Mazumdar* [1989] have the form

$$\mu_e = C\rho_L H \left[\frac{gQ_m}{D} \right]^{1/3}, \quad (11)$$

where ρ_L is the liquid density, g is the acceleration of gravity, Q_m is the airflow rate at middepth, and D is the diameter of the tank. *Mazumdar* [1989] specified the coefficient C to be 4.9×10^{-4} . In the formulation of *Sahai and Guthrie* [1982a], C depends weakly on the tank-averaged void fraction, and we take $C \approx 5.4 \times 10^{-3}$. To evaluate the bulk effective viscosity models and compare the results of the current study and simulations, the eddy diffusivity is assumed to be equal to the (kinematic) eddy viscosity. The eddy diffusivities averaged over the tank and normalized as in (11) are plotted in Figure 11 against a dimensionless source strength [*Asaeda and Imberger*, 1993]:

$$M_H = \frac{gQ_0}{4\pi\alpha_e w_b^3 H}, \quad (12)$$

where Q_0 is the air flow rate at the diffuser, α_e is the entrainment coefficient, and w_b is the bubble slip velocity.

[23] The available data support the bulk effective viscosity models in a few ways (Figure 11). The lack of dependence on the source strength parameter, at least for the results from the present study, *Grevet et al.* [1982], *Sheng and Irons*

[1993], *Sahai and Guthrie* [1982a], and the first case of *Sahai and Guthrie* [1982b], supports the dependence of the bulk effective viscosity on the parameters as given in (11). Also, except for two cases from *Sahai and Guthrie* [1982b], the results are within the range of the predictions of the models. The tank-averaged eddy diffusivity from the present experiments is expected to be an underestimate because no profiles were measured in the bubble plume, where the mixing should be most intense. The *Mazumdar* [1989] model underestimates the bulk effective viscosity, as *Sheng and Irons* [1993] noted, while the *Sahai and Guthrie* [1982a] model either overestimates or provides a good estimate. However, neither model explains the high bulk effective viscosities of two cases from *Sahai and Guthrie* [1982b].

5. Summary

[24] We used the temperature microstructure measurements and calculations of dissipation of turbulent kinetic energy from *Soga and Rehmann* [2004] to compute the dissipation of temperature variance and estimate eddy diffusivities near a bubble plume with two methods from oceanography. Along with the results of SR, these calcu-

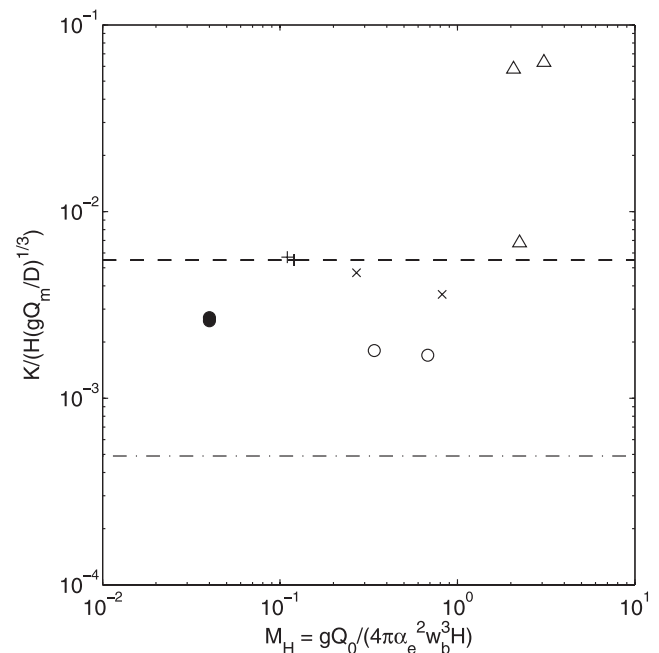


Figure 11. Comparison of the bulk eddy diffusivity from the present study and numerical simulations with the bulk effective viscosity models of *Mazumdar* [1989] and *Sahai and Guthrie* [1982a]. The data symbols are as follows: solid circles, present data; open circles, *Grevet et al.* [1982]; pluses, *Sahai and Guthrie* [1982a]; triangles, *Sahai and Guthrie* [1982b]; crosses, *Sheng and Irons* [1993]. The dashed line represents the bulk effective viscosity model of *Sahai and Guthrie* [1982a], and the dash-dotted line represents the model of *Mazumdar* [1989]. The data are plotted against the source strength parameter M_H from *Asaeda and Imberger* [1993]. When the entrainment coefficient and bubble slip velocity were not reported, we used data from *Wüest et al.* [1992] to estimate $\alpha_e = 0.11$ and $w_b \approx 0.3$ m/s as representative values.

lations form a set of measurements that can be used to test and develop parameterizations for bubble plume turbulence. The spatial variation of the dissipation of temperature variance differed from that of the dissipation of turbulent kinetic energy because of spatial variations in the temperature gradient. The eddy diffusivities showed nonmonotonic behavior with distance from the plume axis, as in numerical simulations. Values of K_T estimated from the equation for temperature variance were comparable to the values of K_ρ estimated from the turbulent kinetic energy equation, but at high $\epsilon/\nu N^2$ the assumed value of the coefficient Γ was too large. Despite the differences in tank dimensions and airflow rate, the magnitude of the eddy diffusivity compared well with the magnitude of the eddy viscosity from numerical simulations. The bulk eddy diffusivity is within the range of values predicted with bulk effective viscosity formulations, which account for differences in tank dimensions and flow rate.

[25] **Acknowledgment.** D.J.W. was supported with a SURGE fellowship from the University of Illinois while this work was done.

References

- Asaeda, T., and J. Imberger (1993), Structure of bubble plumes in linearly stratified environments, *J. Fluid Mech.*, 249, 35–57.
- Barry, M. E., G. N. Ivey, K. B. Winters, and J. Imberger (2001), Measurements of diapycnal diffusivities in stratified fluids, *J. Fluid Mech.*, 442, 267–291.
- Batchelor, G. K. (1959), Small-scale variation of convected quantities like temperature in turbulent fluid, *J. Fluid Mech.*, 5, 113–133.
- Bernard, R. S., R. S. Maier, and H. T. Falvey (2000), A simple computational model for bubble plumes, *Appl. Math. Modell.*, 24, 215–233.
- Efron, B., and R. J. Tibshirani (1993), *An Introduction to the Bootstrap*, 436 pp., CRC Press, Boca Raton, Fla.
- Ellis, C. R., and H. G. Stefan (1991), Field testing of an ice-preserving winter lake aeration system, *Water Resour. Bull.*, 27, 903–914.
- Field, K. M., and E. E. Prepas (1997), Increased abundance and depth distribution of pelagic crustacean zooplankton during hypolimnetic oxygenation in a deep, eutrophic Alberta lake, *Can. J. Fish. Aquat. Sci.*, 54, 2146–2156.
- Gregg, M. C. (1999), Uncertainties and limitations in measuring ϵ and χ_T , *J. Atmos. Oceanic Technol.*, 16, 1483–1490.
- Grevet, J. H., J. Szekely, and N. El-Kaddah (1982), An experimental and theoretical study of gas bubble driven circulation systems, *Int. J. Heat Mass Transfer*, 25, 487–497.
- Heo, W. M., and B. Kim (2004), The effect of artificial destratification on phytoplankton in a reservoir, *Hydrobiologia*, 524, 229–239.
- Iguchi, M., and Z. Morita (1992), The effective viscosity and effective diffusivity of bubbles in an air-water vertical bubbling jet, *ISIJ Int.*, 32, 857–864.
- Iguchi, M., T. Kondoh, Z. Morita, K. Nakajima, K. Hanazaki, T. Uemura, and F. Yamamoto (1995), Velocity and turbulence measurements in a cylindrical bath subject to centric bottom gas injection, *Metall. Mater. Trans. B*, 26, 241–247.
- Imberger, J., and J. C. Patterson (1990), Physical limnology, *Adv. Appl. Mech.*, 27, 303–475.
- Itswire, E. C., K. N. Helland, and C. W. Van Atta (1986), The evolution of grid-generated turbulence in a stably stratified fluid, *J. Fluid Mech.*, 162, 299–338.
- Ivey, G. N., and J. Imberger (1991), On the nature of turbulence in a stratified fluid. Part I: The energetics of mixing, *J. Phys. Oceanogr.*, 21, 651–658.
- Mazumdar, D. (1989), On effective viscosity models for gas-stirred ladle systems, *Metall. Trans. B*, 20, 967–969.
- McGhee, T. J. (1991), *Water Supply and Sewerage*, 602 pp., McGraw-Hill, New York.
- Osborn, T. R. (1980), Estimates of the local rate of vertical diffusion from dissipation measurements, *J. Phys. Oceanogr.*, 10, 83–89.
- Osborn, T. R., and C. S. Cox (1972), Oceanic fine structure, *Geophys. Fluid Dyn.*, 3, 321–345.
- Rehmann, C. R., and T. F. Duda (2000), Diapycnal diffusivity inferred from scalar microstructure measurements near the New England shelf/slope front, *J. Phys. Oceanogr.*, 30, 1354–1371.
- Rehmann, C. R., and J. R. Koseff (2004), Mean potential energy change in weakly and strongly stratified turbulent flow, *Dyn. Atmos. Oceans*, 37, 271–294.
- Rehmann, C. R., D. J. Wain, and L. C. M. Soga (2004), Estimates of the dissipation of turbulent kinetic energy from temperature microstructure, paper presented at World Water and Environmental Resources Congress, Am. Soc. of Civ. Eng., Salt Lake City, Utah.
- Rodi, W. (1987), Examples of calculation methods for flow and mixing in stratified fluids, *J. Geophys. Res.*, 92(C5), 5305–5328.
- Ruddick, B., and T. G. L. Shirtcliffe (1979), Data for double diffusers: Physical properties of aqueous salt-sugar solutions, *Deep Sea Res.*, 26, 775–788.
- Ruddick, B., D. Walsh, and N. Oakey (1997), Variations in apparent mixing efficiency in the North Atlantic Central Waters, *J. Phys. Oceanogr.*, 27, 2589–2605.
- Ruddick, B., A. Anis, and K. Thompson (2000), Maximum likelihood spectral fitting: The Batchelor spectrum, *J. Atmos. Oceanic Technol.*, 17, 1541–1555.
- Sahai, Y., and R. I. L. Guthrie (1982a), Effective viscosity models for gas stirred ladles, *Metall. Trans. B*, 13B, 125–127.
- Sahai, Y., and R. I. L. Guthrie (1982b), Hydrodynamics of gas stirred melts: part II. Axisymmetric flows, *Metall. Trans. B*, 13, 203–277.
- Sander, J., A. Simon, T. Jonas, and A. Wüest (2000), Surface turbulence in natural waters: A comparison of large eddy simulations with microstructure observations, *J. Geophys. Res.*, 105(C1), 1195–1207.
- Schladow, S. G. (1992), Bubble plume dynamics in a stratified medium and the implications for water quality amelioration in lakes, *Water Resour. Res.*, 28, 313–321.
- Sheng, Y. Y., and G. A. Irons (1993), Measurement and modeling of turbulence in the gas/liquid two-phase zone during gas injection, *Metall. Trans. B*, 24, 695–705.
- Smith, B. L. (1998), On the modeling of bubble plumes in a liquid pool, *Appl. Math. Modell.*, 22, 773–797.
- Soga, C. L. M., and C. R. Rehmann (2004), Dissipation of turbulent kinetic energy near a bubble plume, *J. Hydraul. Eng.*, 130, 441–449.
- Tennekes, H., and J. L. Lumley (1989), *A First Course in Turbulence*, 12th ed., 300 pp., MIT Press, Cambridge, Mass.
- Wain, D. J., and C. R. Rehmann (2005), Evaluation of oceanographic microstructure methods for hydraulics problems, paper presented at World Water and Environmental Resources Congress, Am. Soc. of Civ. Eng., Anchorage, Alaska.
- Wüest, A., N. H. Brooks, and D. M. Imboden (1992), Bubble plume modeling for lake restoration, *Water Resour. Res.*, 28, 3235–3250.

C. R. Rehmann and D. J. Wain, Department of Civil, Construction, and Environmental Engineering, Iowa State University, Ames, IA 50011, USA. (rehmann@iastate.edu)